

Impact of Antecedent Soil Moisture Anomalies over the Indo-China Peninsula on the Super Meiyu Event in 2020

Yinshuo DONG^{1,2}, Haishan CHEN^{1,2*}, and Xuan DONG^{1,2}

¹ Key Laboratory of Meteorological Disaster, Ministry of Education/Joint International Research Laboratory of Climate and Environment Change/Collaborative Innovation Center on Forecast and Evaluation of Meteorological Disasters, Nanjing University of Information Science & Technology, Nanjing 210044

² School of Atmospheric Sciences, Nanjing University of Information Science & Technology, Nanjing 210044

(Received 16 September 2022; in final form 11 November 2022)

ABSTRACT

In the summer of 2020, a super Meiyu event occurred in the Yangtze River basin (YRB), causing enormous economic losses and human casualties. Recent studies have investigated the possible causes of this super Meiyu event from the perspective of anomalous atmospheric circulation activities and sea surface temperature (SST) anomalies; however, the influence of land surface processes has not garnered considerable attention. This study investigates the possible contributions of land surface processes to this extreme event based on observational analysis and numerical simulations, and shows that antecedent soil moisture (SM) anomalies over the Indo-China Peninsula (ICP) may have had a vital influence on the super Meiyu in 2020. Negative SM anomalies in May over the ICP increased the surface temperature and sensible heat flux. The “memory” of soil allowed the anomalies to persist into the Meiyu period. The heating of the lower atmosphere by the surface strengthened the western Pacific subtropical high, which caused an anomalous anticyclone from the ICP to Northwest Pacific and thus enhanced the southwesterly winds and vertical motion over the YRB. Consequently, the water vapor flux and convergence were strengthened. Sensitivity experiments based on the Weather Research and Forecasting (WRF) model further confirmed the results of observational analysis and indicated that the warm air heated by the ICP surface significantly warmed the lower troposphere from the ICP to Northwest Pacific under the influence of the background wind, thus increasing the geopotential height and inducing an anticyclone. The results of the sensitivity experiments showed that the SM anomalies in May over the ICP increased the precipitation by 10.6% from June to July over the YRB. These findings can improve our understanding of the mechanism of the super Meiyu event in 2020 and facilitate the prediction of extreme Meiyu events.

Key words: super Meiyu, soil moisture, Indo-China Peninsula, surface heating

Citation: Dong, Y. S., H. S. Chen, and X. Dong, 2023: Impact of antecedent soil moisture anomalies over the Indo-China Peninsula on the super Meiyu event in 2020. *J. Meteor. Res.*, **37**(2), 234–247, doi: 10.1007/s13351-023-2144-4.

1. Introduction

Meiyu is a unique rainy season during the East Asian summer monsoon (EASM). From mid-June to mid-July each year, the Meiyu front is maintained from the Yangtze River basin (YRB) in China to southern Japan. A rain belt is established along the YRB, Korean Peninsula, and Japan, providing most of the annual precipitation for these regions (Ding and Chan, 2005; Tao and Wei, 2006; Ding et al., 2007, 2018). In the summer of 2020, the YRB experienced a Meiyu event with a record-

breaking duration over the last 30 years. The precipitation accumulated in the Meiyu event of 2020 was far more than those of 1998 and 2016 (Guo et al., 2016; Bao, 2021). Characterized by an early onset, a late retreat, and frequent heavy rainfall, this super Meiyu event led to a historic flooding disaster and caused huge economic losses (Liu and Ding, 2020; Zhang et al., 2020; Ding et al., 2021). Water vapor transport is an important factor regulating the precipitation intensity. By analyzing the water vapor source and transport process of this super Meiyu event, Zhang L. X. et al. (2021) found that local

Supported by the National Key Research and Development Program of China (2022YFF0801603).

*Corresponding author: haishan@nuist.edu.cn

© The Chinese Meteorological Society and Springer-Verlag Berlin Heidelberg 2023

evaporation and water vapor transport from the Indian monsoon region were considerably higher than normal. Wang et al. (2021) indicated that atmospheric rivers associated with jet streams continuously supplied water vapor for the Meiyu event in 2020. Notably, some studies suggested that Indian Ocean (IO) warming plays an important role in the record-breaking Meiyu event (Takaya et al., 2020; Ding et al., 2021; Fang et al., 2021; Zhou et al., 2021). Zhou et al. (2021) found that anomalous IO sea surface temperature (SST) could strengthen the anti-cyclone over Northwest Pacific and enhance the westward extension of the western Pacific subtropical high (WPSH), thereby providing favorable conditions for the development of the super Meiyu event. Zhang W. J. et al. (2021) further suggested that the long-lasting and quasi-stationary Madden–Julian oscillation over the IO contributed to the Meiyu process in 2020. Liu et al. (2020) stated that the North Atlantic Oscillation enhanced the subseasonal processes of the Meiyu front. However, few studies have focused on the impact of land surface processes on this record-breaking Meiyu event.

As the land surface is the lower boundary of the atmosphere, complex momentum, energy, and mass exchanges occur between the land and atmosphere. Land surface factors, such as soil moisture (SM) and snow cover, can exert local or non-local effects on the atmosphere by modulating the surface radiation, energy, and water balance (Seneviratne et al., 2006, 2010; Dirmeyer et al., 2009; Chen et al., 2022). For instance, Zhang and Zuo (2011) found that the negative SM in spring over East and North China could reduce the land–sea temperature difference and thus weaken the EASM. Gao et al. (2014) revealed that the SM in Southwest China is significantly correlated with summer precipitation in the YRB. The Indo-China Peninsula (ICP), the Southernmost continent in East Asia, is located upstream of the EASM region. Several studies have indicated that the state of the land surface of the ICP has a critical impact on the formation and development of the EASM (Shi et al., 2008; Gao et al., 2019, 2020b). According to Chow et al. (2006), the thermal condition of the ICP can strongly impact the intensity of the subtropical high, and surface heating over the ICP has a non-negligible effect on the monsoon circulation and precipitation. Zhuang et al. (2022) demonstrated the key role of land surface processes over the ICP in summer monsoon processes using the atmospheric general circulation model.

As a key factor of land surface processes, SM can regulate surface heat fluxes by affecting evapotranspiration, and its “memory” allows anomalies to be maintained on monthly to seasonal scales (Koster and Suarez, 2001;

Dirmeyer et al., 2009). Gao et al. (2020b) found a significant negative correlation between the spring SM anomalies in the ICP and summer precipitation in the YRB. The spring SM in the ICP is also closely related to heat extremes over the YRB (Yang et al., 2019). Dong et al. (2022a) suggested that SM in the ICP significantly influences the local precipitation and precipitation in South China (SC).

All the above studies show that SM anomalies over the ICP land surface can exert local and non-local impacts by substantially altering the atmospheric circulation. However, the influence of land surface processes on the super Meiyu event in 2020 has not received much attention. Therefore, we aimed to investigate the precursory signals of land surface processes over the ICP before the onset of the super Meiyu even in 2020 and their possible physical mechanisms. The remainder of this study is organized as follows. The data and methods are presented in Section 2. In Section 3, we examine the relationship between the super Meiyu event in 2020 and the SM anomalies over the ICP in May 2020. Section 4 presents the results of the numerical sensitivity experiments and verifies the possible physical mechanisms for this relationship through in-depth analysis. The conclusions and discussion are presented in Section 5.

2. Data and methods

2.1 Data

Daily precipitation observation data from approximately 2420 weather stations in China during 1991–2020 were provided by the China Meteorological Administration. The fifth-generation ECWMF reanalysis (ERA-5) data (Hersbach et al., 2020) assimilates a large amount of conventional observations and satellite data, and contains long time-series and high-resolution data. The ERA-5 dataset is available from <https://www.ecmwf.int>. Atmospheric variables, including the geopotential height, wind, temperature, and vertical velocity, were obtained from monthly ERA-5 data from 1991 to 2020, with a spatial resolution of $0.25^\circ \times 0.25^\circ$. We utilized the land surface elements of ERA-5, including the hourly and monthly averaged SM (0–7 cm), surface temperature, surface sensible heat flux, and surface latent heat flux, with a spatial resolution of $0.1^\circ \times 0.1^\circ$ from 1991 to 2020. The merged multi-satellite surface SM dataset developed by the European Space Agency (ESA) in the Climate Change Initiative (CCI) project (ESA-CCI combined SM v06.1, hereafter referred to as ESA-CCI; Dorigo et al., 2017) is available at <https://www.esa-soilmoisture-cci.org>. This daily dataset spans from 1991

to 2020, with a spatial resolution of $0.25^\circ \times 0.25^\circ$ and a thickness of ~ 2 cm. Moreover, we also adopted the monthly product generated by the Noah model in the Global Land Data Assimilation System (GLDAS; Rodell et al., 2004), which can be downloaded from <https://ldas.gsfc.nasa.gov/gldas>. The variables used in this study include SM (0–10 cm), surface temperature, surface sensible heat flux, and surface latent heat flux with a horizontal resolution of $0.25^\circ \times 0.25^\circ$; these variables were combined with the data from GLDASv2.0 for 1991–1999 and GLDASv2.1 for 2000–2020 to form a time series to be used as other datasets. All data from 1991 to 2020 were selected to obtain climatological means.

2.2 Methods

The Singular Value Decomposition (SVD) technique (Bretherton et al., 1992; Wallace et al., 1992) was used to analyze the relationship between SM anomalies in May over the ICP and precipitation from June to July in the YRB. This method has been widely used in meteorological research and therefore is not introduced here to avoid redundancy (Zhang and Zuo, 2011; Lin et al., 2019; Dong et al., 2022b). Additionally, the SM and precipitation data were linearly detrended and standardized before conducting SVD.

2.3 Model

Numerical experiments were conducted by using the Weather Research and Forecasting (WRF) model version 4.3, which is a land-atmospheric coupled model developed through a partnership between the NCEP, NCAR, and several other research institutions. The source code of the WRF model was obtained from <https://www2.mmm.ucar.edu/wrf/users/download/>. All

the experiments were configured with a single domain, which used the Lambert projection on horizontal grids with a size of $50\text{ km} \times 50\text{ km}$ (Fig. 1a). The initial and boundary conditions of the model were obtained from the Final Reanalysis Data (FNL) jointly developed by NCEP/NCAR with a spatial resolution of $1^\circ \times 1^\circ$ and a temporal resolution of 6 h. The Community Land Model version 4 (CLM4; Dai et al., 2003; Oleson et al., 2010; Lawrence et al., 2011), Rapid Radiative Transfer Model for General Circulation Models (GCMs; Iacono et al., 2008), Yonsei University planetary boundary layer scheme (Hong et al., 2006), WRF single-moment six-class microphysics scheme (Hong and Lim, 2006), and new Tiedtke scheme (Zhang and Wang, 2017) were applied to all experiments. In CLM4, the land surface in each model grid cell had a soil column of 10 layers at depths ranging from the surface to 3.433 m.

2.4 Experimental design

In the control experiments (CTRL), no changes were made to the model, implying that the SM was freely coupled with other variables. As the model is sensitive to the initial field and requires several days to adjust from the initial conditions to the equilibrium state, all results of the experiments were averaged from eight different initial times (0000 UTC, 0600 UTC, 1200 UTC, 1800 UTC 26 April, 0000 UTC, 0600 UTC, 1200 UTC, and 1800 UTC 27 April) to 1800 UTC 31 July 2020.

In the sensitivity experiments (CLIM), the SM in the first three layers (0–9.1 cm) of each grid cell over the ICP (red box in Fig. 1a, $10^\circ\text{--}20^\circ\text{N}$, $97^\circ\text{--}110^\circ\text{E}$) in May was prescribed to the daily climatological mean calculated from the ERA-5 data during 1991–2020 (black line in Fig. 1b). In this way, the anomalous circulation due to the SM in May over the ICP could be obtained by sub-

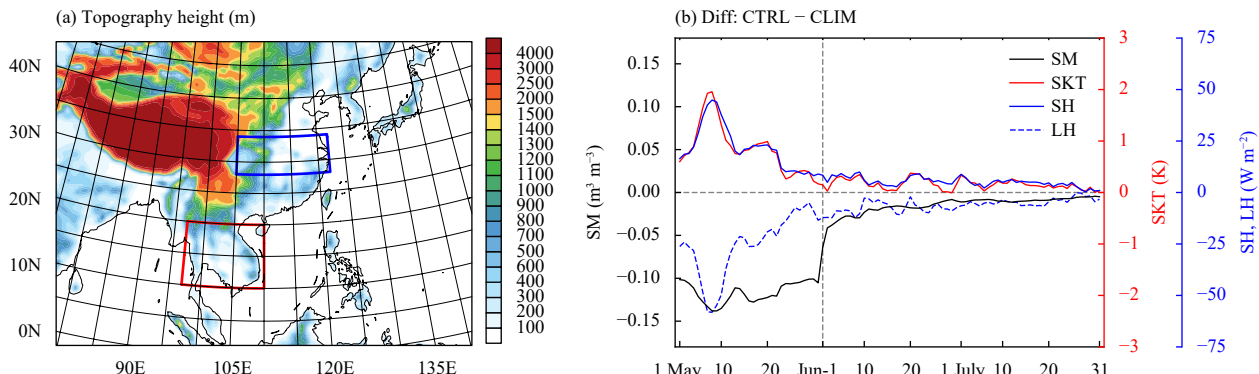


Fig. 1. (a) Terrain height (m) over the WRF model domain. The red box denotes the ICP ($10^\circ\text{--}20^\circ\text{N}$, $97^\circ\text{--}110^\circ\text{E}$), whose SM was prescribed in sensitivity experiments, and the blue box denotes the YRB region ($28^\circ\text{--}34^\circ\text{N}$, $105^\circ\text{--}122^\circ\text{E}$). (b) The soil moisture (SM, black solid line; $\text{m}^3 \text{m}^{-3}$), surface temperature (SKT, red solid line; K), surface sensible heat flux (SH, blue solid line; W m^{-2}), and surface latent heat flux (LH, blue dashed line; W m^{-2}) averaged over the ICP obtained by subtracting CLIM from CTRL from 1 May to 31 July 2020.

tracting CLIM from CTRL. The first three layers of SM outside the ICP in May were set as the daily average obtained from CTRL to ensure that the precipitation anomalies from June to July were solely caused by the SM anomalies in May over the ICP. The other parameters of CLIM were the same as those in CTRL, and Student's *t*-test was applied to check the significance of the differences between ensembles.

3. Relationship between super Meiyu event in 2020 and preceding land surface factors

Figure 2a shows the daily and accumulated precipitation from 1 June to 31 July in the YRB region over the past 30 years. In June and July 2020, approximately two-thirds of the daily precipitation exceeded the climatological mean, wherein the multi-day precipitation reached 20 mm day^{-1} . The accumulated precipitation (red line in **Fig. 2a**) was approximately twice the climatological value (black line in **Fig. 2a**), and was much higher than that during the same period in previous years (gray lines in **Fig. 2a**). **Figure 2b** shows the anomalies of precipitation and circulation from 1 June to 31 July 2020, and anomalous positive precipitation was observed in the YRB. Obvious positive geopotential height anomalies and an anticyclone can be found from SC to Northwest Pacific during this period, and the precipitation is suppressed in SC as this region is controlled by the anticyclone. **Figure 2c** shows the spatial distribution of vertical motion and circulation anomalies. Under the impact of the subtropical high, a descending motion occurred from SC to Northwest Pacific. Meanwhile, the convergence of the wind over the YRB resulted in an ascending motion, which was conducive to local precipitation.

The anomalies of water vapor convergence and flux vertically integrated from 1000 to 300 hPa are shown in **Fig. 2d**. The southwest wind in the northwest quadrant of the anomalous anticyclone transported sufficient water vapor to the YRB (**Fig. 2d**), which was favorable for precipitation. As shown by the anomalies of temperature and geopotential height at 850 hPa in **Fig. 2e**, the distribution of the anticyclone and geopotential heights is similar to that of the upper level (**Figs. 2b, c**), indicating an equivalent barotropic structure. Warm anomalies stretch from the ICP to Northwest Pacific, whereas cold anomalies are located north of the Yangtze River. A strong temperature gradient corresponds to the persistently strong Meiyu front. The convergence of cold and warm air is conducive to the formation and development of persistent frontal precipitation.

The SM, surface temperature, surface sensible heat

flux, and surface latent heat flux over the ICP averaged from May and June to July 2020 are shown in **Fig. 3**. As the results of land surface elements are sensitive to the datasets (Seneviratne et al., 2010; Gu et al., 2019; Li et al., 2021; Dong et al., 2022a), the ERA-5 and GLADS datasets were used for comparison. A significant negative SM anomaly was observed over the ICP in May 2020 (**Figs. 3a, i**) in both datasets. Owing to the “memory” of SM, the anomaly lasted until June and July (**Figs. 3e, m**). From May to July, the skin temperature over the ICP remained positive in both datasets (column 2 in **Fig. 3**), which was accompanied by a positive surface sensible heat flux (column 3 in **Fig. 3**). The surface latent heat flux was negative in May (**Figs. 3d, l**) but positive from June to July (**Figs. 3h, p**). Dirmeyer et al. (2009) and Seneviratne et al. (2010) indicated that when SM and evapotranspiration are negatively correlated, evapotranspiration controls SM, implying that stronger evapotranspiration results in a lower SM. When they are positively correlated, SM controls evapotranspiration, namely, a higher SM leads to stronger evapotranspiration. The ICP shows negative latent heat flux anomalies in May, which indicates that evapotranspiration was limited by the dry soil, and the atmosphere was mainly heated by the sensible heat flux. Meanwhile, the positive latent heat flux anomalies in June and July indicated enhanced evapotranspiration. **Figure 3** shows that negative SM anomalies and positive temperature anomalies in May could persist into the Meiyu season, and prolonged surface warming could heat the lower troposphere, thus resulting in an increase in temperature and geopotential height (**Fig. 2e**). Gao et al. (2020b) also suggested that SM in spring over the ICP is significantly correlated with the summer precipitation in the YRB, and surface heating caused by negative SM anomalies is conducive to the westward extension of the WPSH in summer.

To further confirm the robustness of such historical relationships, SVD analysis was conducted on the SM anomalies in May over the ICP and the average June–July precipitation anomalies in the YRB from 1991 to 2020. **Figure 4** shows the first mode of the SVD results. This mode explains approximately 60% of the total covariance, and the correlation coefficient between the expansion coefficients of the left and right fields of this mode is $0.63 (p < 0.01)$ (**Fig. 4c**). The heterogeneous maps (**Figs. 4a, b**) demonstrate the relationship between SM in May and precipitation in June and July. Notably, when the SM in May over the ICP is in the negative phase, precipitation in the YRB from June to July is in the positive phase, suggesting a significant negative correlation between them. Owing to the differences among the SM

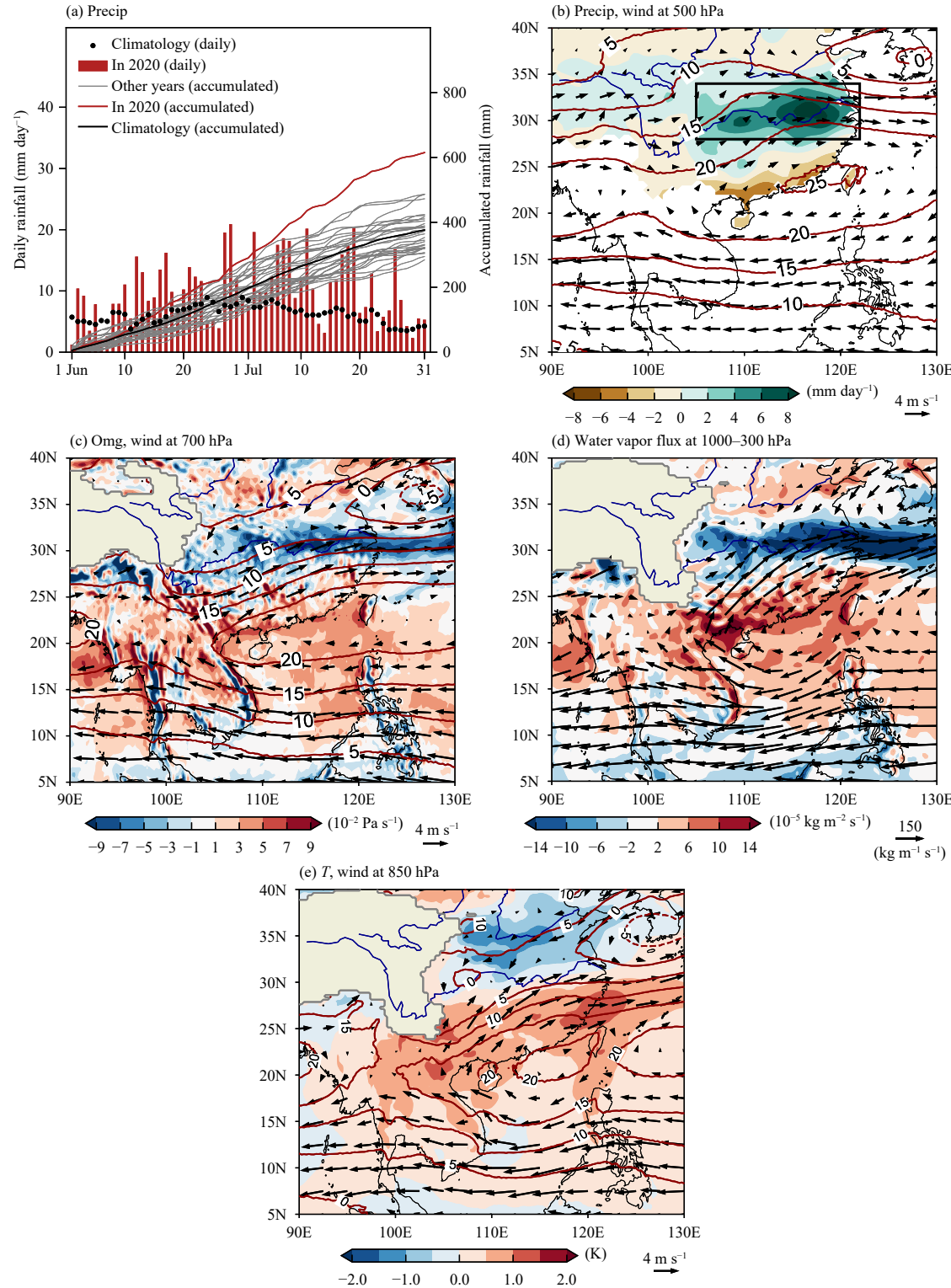


Fig. 2. (a) Daily precipitation in 2020 (red bar; mm day^{-1} ; left y-axis), daily accumulated precipitation since 1 June 2020 (red line; mm; right y-axis), climatological daily precipitation (black dot; mm day^{-1} ; left y-axis), and climatological daily accumulated precipitation (black line; mm; right y-axis) over the YRB (black box in Fig. 2b). Gray lines indicate the annual daily accumulated precipitation in other years from 1991 to 2019 (mm; right y-axis) over the YRB. Spatial distributions averaged from 1 June to 31 July 2020 of (b) anomalies of precipitation (shaded; mm day^{-1}), wind at 500 hPa (vector; m s^{-1}), and geopotential height at 500 hPa (contour; gpm); (c) anomalies of vertical velocity (shaded; $10^{-2} \text{ Pa s}^{-1}$), wind (vector; m s^{-1}), and geopotential height (contour; gpm) at 700 hPa; (d) anomalies of water vapor flux (vector; $10^{-5} \text{ kg m}^{-2} \text{ s}^{-1}$) and convergence (shaded; $10^{-5} \text{ kg m}^{-1} \text{ s}^{-1}$) integrated from 1000 to 300 hPa; and (e) anomalies of temperature (shaded; K), wind (vector; m s^{-1}), and geopotential height (contour; gpm) at 850 hPa.

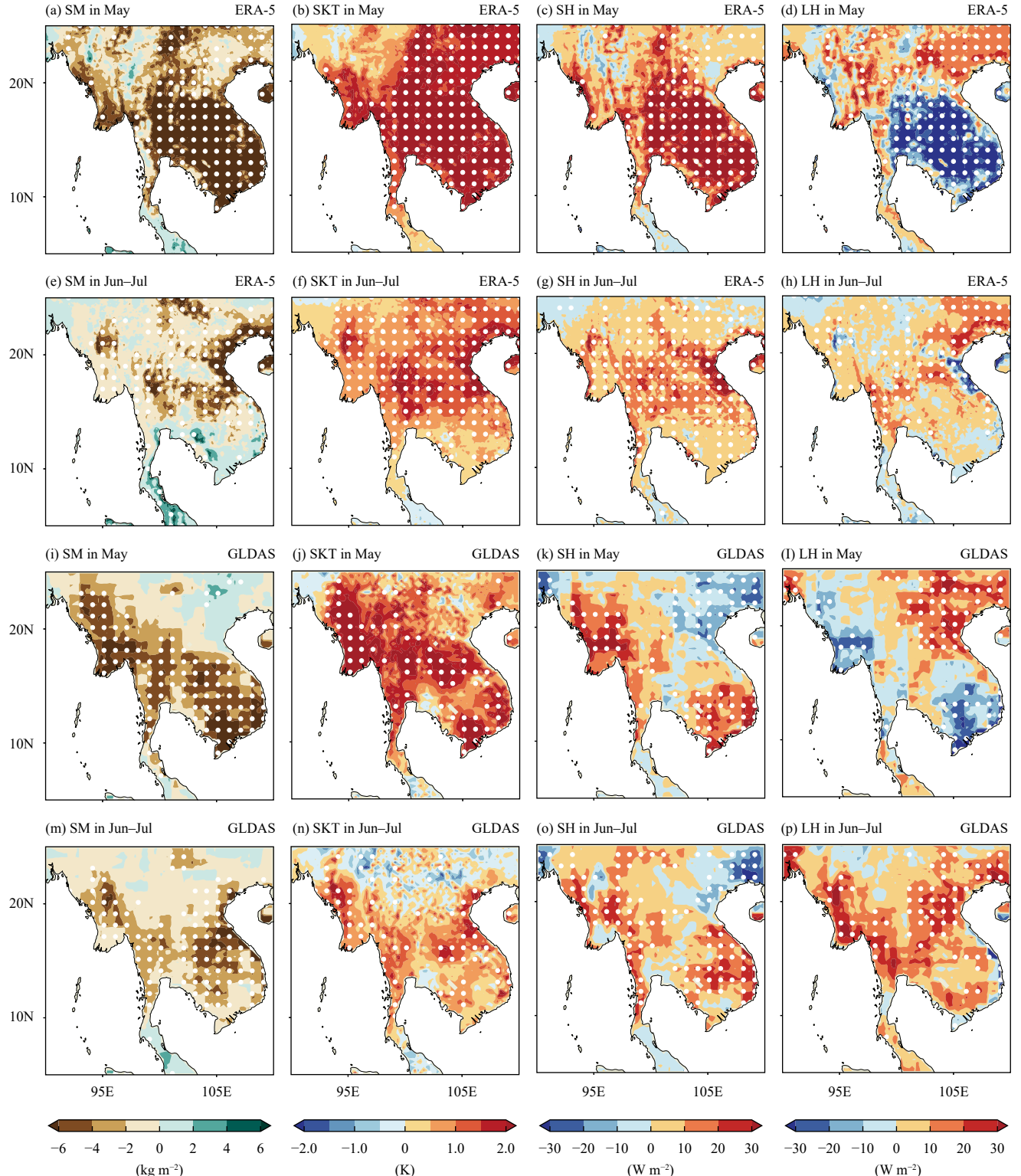


Fig. 3. Anomalies of (a, e, i, m) soil moisture (SM, shaded; $\text{m}^3 \text{m}^{-3}$), (b, f, j, n) surface temperature (SKT, shaded; K), (c, g, k, o) surface sensible heat flux (SH, shaded; W m^{-2}), and (d, h, l, p) surface latent heat flux (LH, shaded; W m^{-2}) in May 2020 over the ICP, calculated from the (a–h) ERA-5 and (i–p) GLDAS data. The white dotted areas indicate anomaly values that are greater than the standard deviations.

datasets, Fig. 4d shows the comparison of the standard-
ized time series of ERA-5, GLDAS, and ESA-CCI data
averaged over the ICP region ($10^\circ\text{--}20^\circ\text{N}$, $97^\circ\text{--}110^\circ\text{E}$, the

black box in Fig. 4a) for May during 1991–2020. The correlation coefficient between the time series of ERA-5 and ESA-CCI data is 0.86 ($p < 0.01$), and that between

the time series of ERA-5 and GLDAS data is 0.90 ($p < 0.01$), thus suggesting a high correlation and consistency in the interannual variability of different datasets.

The SM in May over the ICP (black box in Fig. 4a) from 1991 to 2020 was further standardized and averaged regionally to obtain a time series of 30 yr. For a better demonstration, this time series was multiplied by -1 to obtain the SM index of the ICP. To obtain the precipitation index, the June–July precipitation in the YRB (black box in Fig. 4b) from 1991 to 2020 was standardized and averaged regionally. The correlation coefficient between the SM (precipitation) index and the expansion coefficients of the left (right) field in the SVD results (Fig. 4c) is 0.98 (0.71) ($p < 0.01$), and that between the two indices is 0.39 ($p < 0.05$). Thus, these two indices can represent the elements of the original field owing to the significant correlation between them.

The 700-hPa geopotential height and wind averaged from June to July were regressed onto the ICP SM index in May (Fig. 5a). Notably, an obvious anticyclone is located from Northwest Pacific to the ICP, and the positive

geopotential height anomalies extend westward to the ICP. The regressed water vapor flux and convergence vertically integrated from 1000 to 300 hPa are shown in Fig. 5b. The anticyclonic water vapor flux with a center over the South China Sea (SCS) and the enhanced water vapor convergence increased the transfer of water vapor to the YRB. Under the control of the anomalous anticyclone, the precipitation decreased in SC. The regression results for 1991–2020 shown in Fig. 5 are consistent with the anomaly fields in 2020 (Figs. 2c, d), thus confirming the significant negative correlation between the SM anomalies in May over the ICP and the precipitation in June and July over the YRB. The relevant mechanism for this relationship might be that the negative SM anomalies over the ICP lead to increases in the land surface temperature and sensible heat flux from the surface to the atmosphere, thereby warming up the lower atmosphere and elevating the geopotential height. This can facilitate the westward extension of the WPSH and the anomalous anticyclone from the SCS to Northwest Pacific. Meanwhile, the water vapor flux and convergence were en-

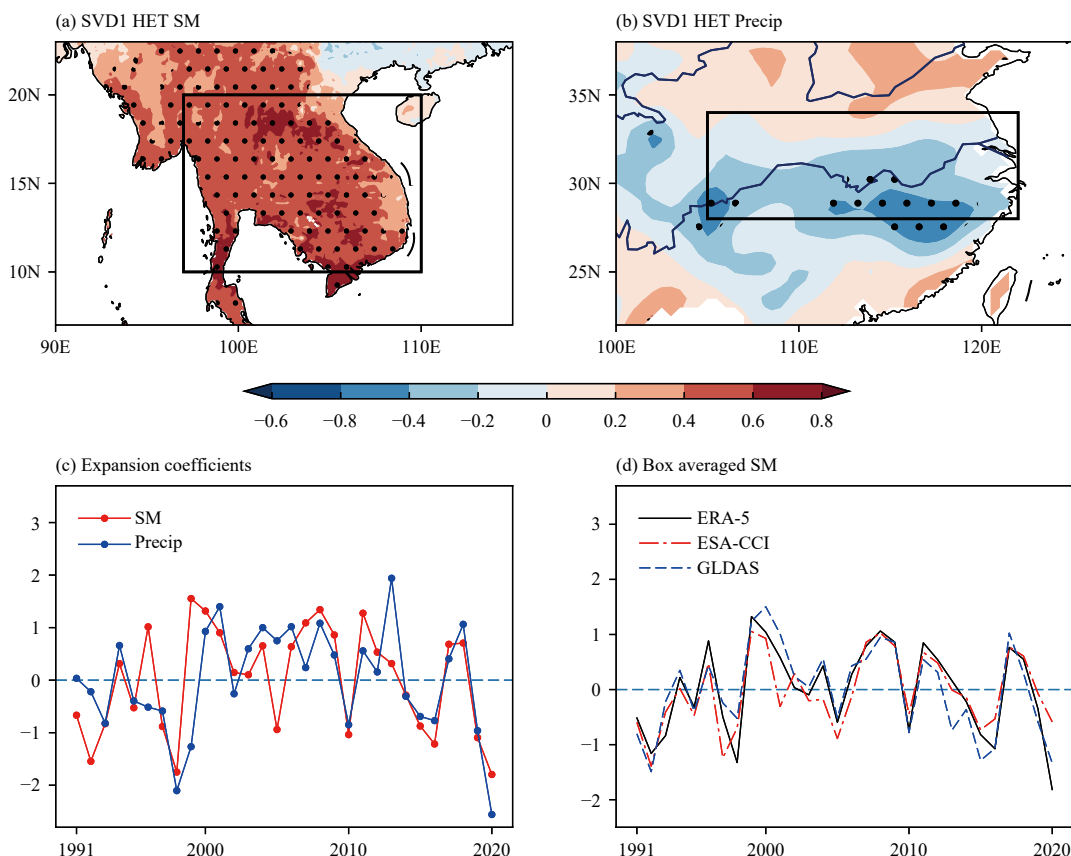


Fig. 4. First SVD mode of heterogeneous maps between (a) the SM in May and (b) precipitation during June and July. The black dotted areas are significant at the 5% significance level. (c) The expansion coefficients of the first SVD mode. (d) Time series of the standardized regional average SM over the ICP (black box in Fig. 4a) based on the ERA-5 (black solid line), ESA-CCI (red dash dotted line), and GLDAS (blue dashed line) data. All data are linearly detrended and standardized for the period of 1991–2020 before SVD analysis.

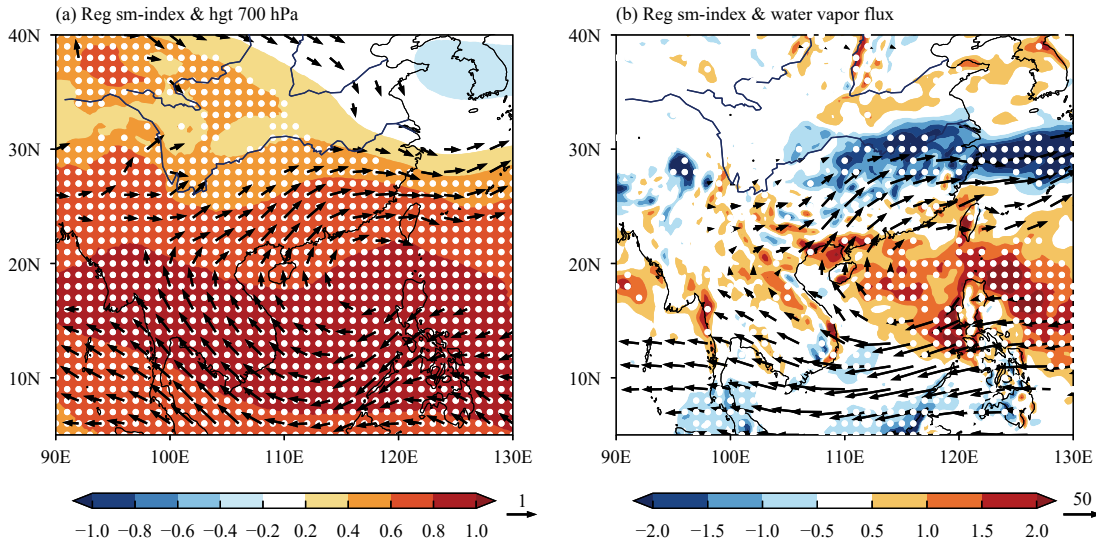


Fig. 5. Regression of (a) wind (vector) and geopotential height (shaded) at 700 hPa and (b) water vapor convergence (shaded) and water vapor flux (vector) vertically integrated from 1000 to 300 hPa in June and July to the standardized SM index in May. The white dotted areas are significant at the 5% level. All data are linearly detrended and standardized before the regression analysis from 1991 to 2020.

hanced over the YRB, which might be the cause of the precipitation increase during the Meiyu period of 2020.

However, a clear mechanism for the impact of SM on precipitation cannot be derived from the correlation alone, because precipitation is influenced by many other factors. Thus, the next section introduces the numerical simulations and sensitivity experiments conducted by modifying the SM in the ICP in the WRF model, and the results can further identify the relevant physical mechanism of the impact of SM on precipitation.

4. Numerical simulations and analysis of the related physical mechanism

4.1 Model evaluation

Figure 6 shows the comparison of the differences between CTRL and the reanalysis data based on the ERA-5 wind, geopotential height, and observational precipitation data described in Section 2 from May to July 2020. Notably, the model reproduces the precipitation areas in SC and southern Tibetan Plateau in May 2020, but the simulated precipitation is higher (Figs. 6a–c). Similarly, from June to July, a bias is observed in the simulated precipitation on the south Tibetan Plateau (Fig. 6f). This is probably because the model is sensitive to the steep terrain and mountains (Fig. 1a). This type of model bias has been reported in previous studies (Wang et al., 2013; Zhang et al., 2016; Dong et al., 2022a). From June to July, the CTRL satisfactorily reproduced the distribution of the rain belt and circulation in the YRB, but slightly underestimated the geopotential height (Figs.

6d–f). Overall, the model can capture the main features and variations of the East Asian atmospheric circulation during May–July 2020 and reproduce the intensity and spatial distribution of precipitation in the study area. Therefore, sensitivity experiments can be conducted based on CTRL to verify the aforementioned physical processes.

4.2 Results of sensitivity experiments and the possible physical processes

In the CLIM experiments, the SM in May 2020 over the ICP (red box in Fig. 1a) was fixed as the daily climatological mean. The land surface and atmosphere were freely coupled in June and July. Therefore, the impact of the SM anomalies in May on the atmosphere can be obtained by subtracting CLIM from CTRL. Figure 1b shows the daily variations of the differences in land surface elements between the CTRL and CLIM experiments from May to July. Notably, in May, the SM value is obviously lower than the climatological mean, and the daily variations in surface temperature, surface sensible heat flux, and surface latent heat flux are clearly consistent with the variations in SM. In June and July, the difference in SM between CTRL and CLIM gradually decreased as a result of land–atmosphere interaction. Owing to the “memory” feature of SM, the SM of the ICP in CTRL is still lower than that in CLIM from June to July, and the negative SM anomalies lead to an increase in the surface temperature and an increase (decrease) in the sensible (latent) heat flux. The special distributions of the differences between CTRL and CLIM in May 2020 are

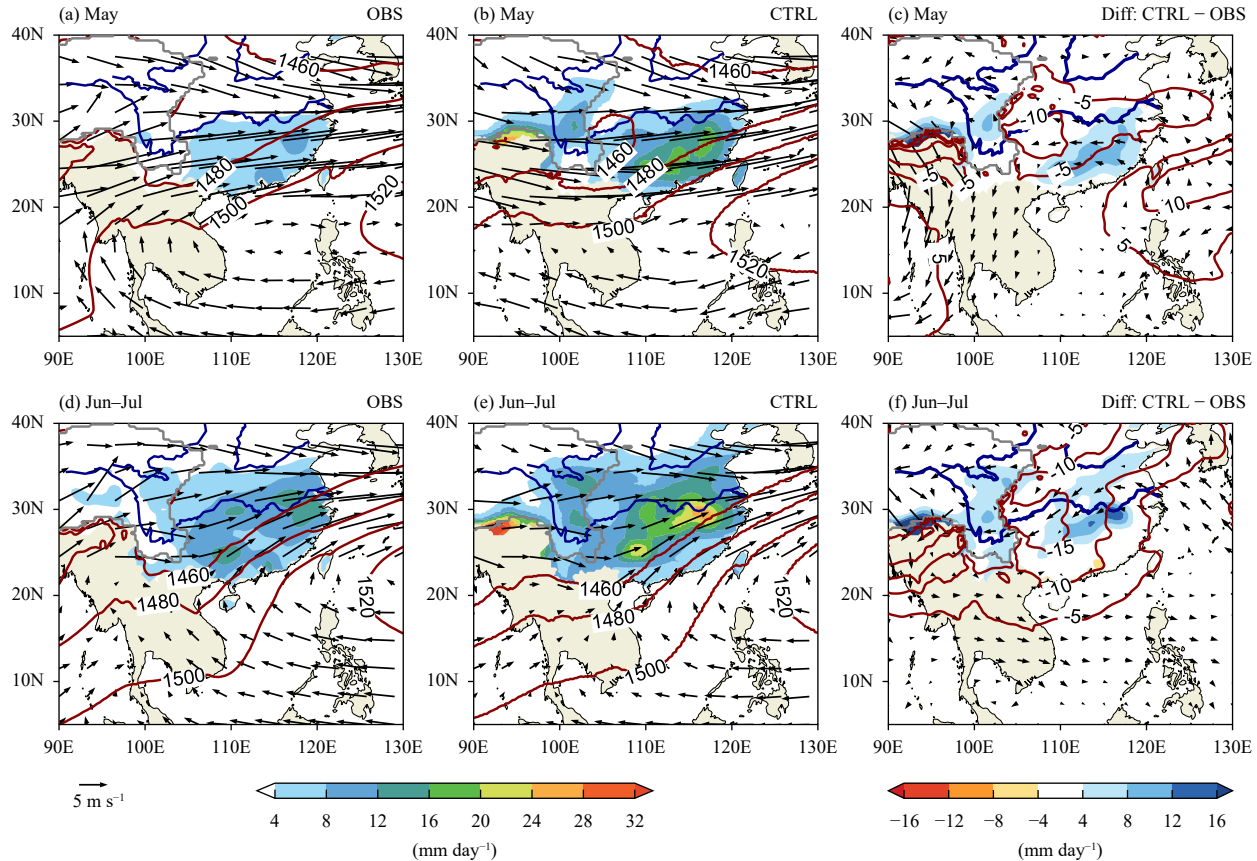


Fig. 6. (a) Daily precipitation (shaded; mm day^{-1}), 850-hPa geopotential height (red contour; gpm), and 500-hPa wind (vector; m s^{-1}) in the (a, d) observation and (b, e) CTRL, and (c, f) their differences of reanalysis datasets. The gray solid lines represent the Tibetan Plateau region.

shown in Fig. 7. A significantly negative difference in the SM (Fig. 7a) and a positive difference in the surface temperature were observed over the ICP (Fig. 7b). The increase in the sensible heat flux (Fig. 7c) and decrease in the latent heat flux (Fig. 7d) indicate that dry soil can result in a positive surface temperature. The results obtained by subtracting CLIM from CTRL are consistent with the reanalysis data (Fig. 3).

The spatial distributions of daily precipitation and wind from 1 June to 31 July 2020, obtained by subtracting CLIM from CTRL, are shown in Fig. 8a. Obvious positive precipitation anomalies can be observed from the YRB to the southern part of Japan, and the distribution of precipitation is similar to that of the narrow rain belt in East Asia during the Meiyu event. SC experienced decreased precipitation under the control of an anticyclone. The distributions of circulation and precipitation were consistent with those of the observation and reanalysis data shown in Fig. 2b. Figure 8b shows the differences in the vertical velocity (ω) between CTRL and CLIM from 1 June to 31 July 2020. A strong ascending motion occurs corresponding to the location of the rainbelt, and SC is dominated by a descending motion

under the control of the anticyclone. Overall, the CLIM reproduced the distribution of the vertical velocity in the reanalysis data (Fig. 2c). Figure 8c further analyzes the water vapor flux and convergence integrated from 1000 to 300 hPa. An evident water vapor convergence exists in the YRB, which is supported by sufficient water vapor transported along the southwesterly winds. The model results were consistent with the water vapor flux and convergence calculated from the reanalysis data (Fig. 2d).

The 850-hPa temperature and geopotential height in June–July 2020 were further analyzed, as shown in Fig. 8d. Significant warming occurs from the ICP to Northwest Pacific, and anticyclonic and positive geopotential height anomalies occur consistently between 850 and 500 hPa, suggesting that increased land surface temperature can heat the lower troposphere and increase the geopotential height. Gao et al. (2020c) found a similar response through numerical simulations with increased low-level temperature over the ICP and suggested that the non-adiabatic heating of the ICP has a critical effect on the form of a subtropical high. However, in the CLIM, the heating owing to prescribed SM anomalies is con-

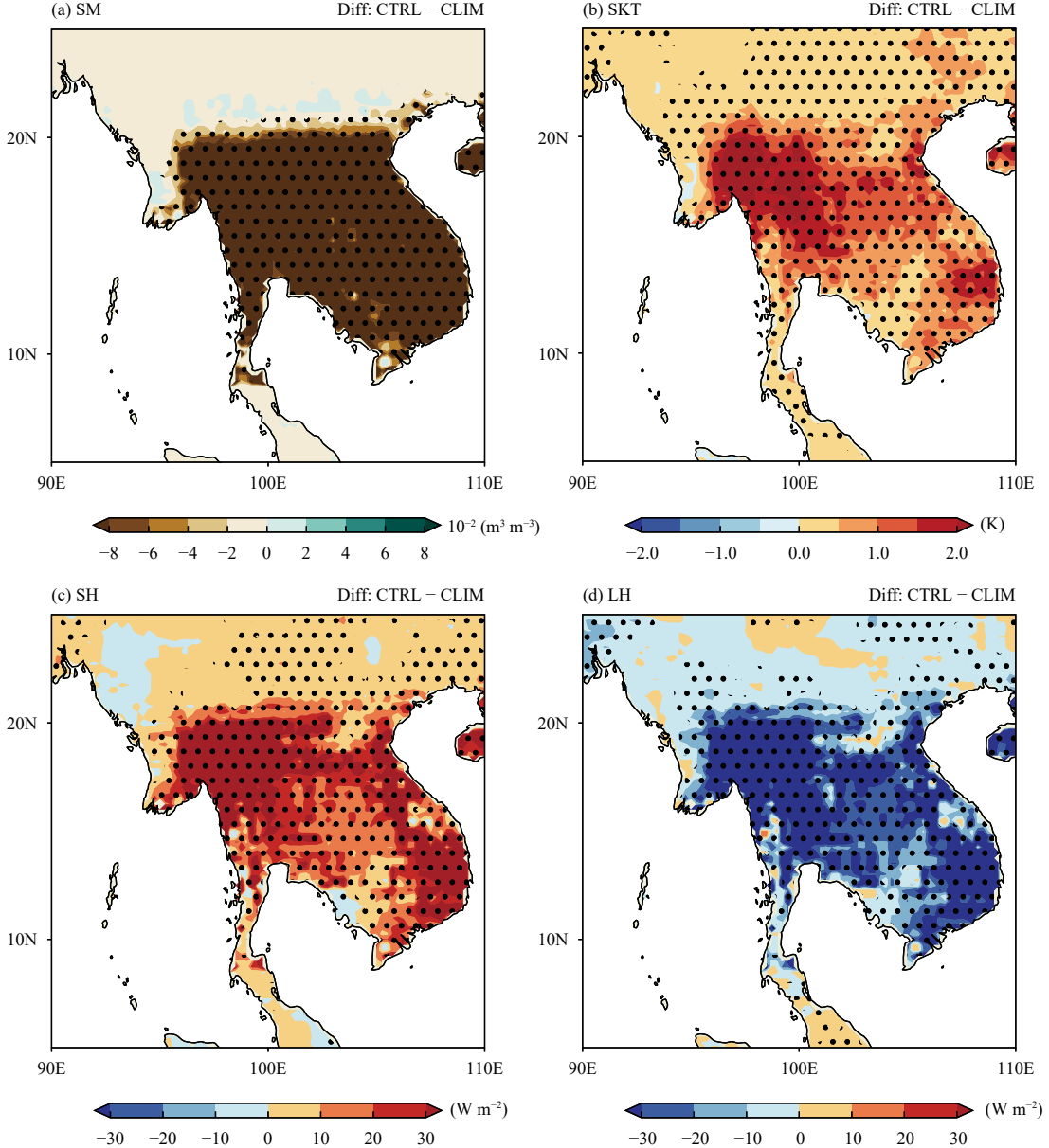


Fig. 7. (a) Soil moisture (SM, shaded; $10^{-2} \text{ m}^3 \text{ m}^{-3}$), (b) surface temperature (SKT, shaded; K), (c) surface sensible heat flux (SH, shaded; W m^{-2}), and (d) surface latent heat flux (LH, shaded; W m^{-2}) in May 2020 over the ICP obtained by subtracting CLIM from CTRL. The black dotted areas are significant at the 5% level.

fined to the surface of the ICP. The warm air heated by the surface is advected downstream to SC and Northwest Pacific due to the background southwesterly winds (Figs. 6b, e), thus producing non-local effects. Apart from increasing the geopotential height, warm advection also creates a strong temperature gradient with cold air over the YRB. Gao et al. (2020b) applied the vertical motion (omega) equation and found that warm advection from the ICP favors enhanced vertical motion in the YRB. The distribution of temperature and geopotential height in the CLIM is generally consistent with that shown in Fig. 2e. The above analysis of the sensitivity experiments veri-

fies the physical processes described in Section 3.

The possible contribution of SM anomalies in May over the ICP to the precipitation in June and July over the YRB was further quantified through sensitivity experiments. The simulation results show that the average daily precipitation values in June–July in the YRB ($28^\circ\text{--}34^\circ\text{N}$, $105^\circ\text{--}122^\circ\text{E}$) obtained from CTRL and CLIM are 11.67 and $10.43 \text{ mm day}^{-1}$, respectively. The difference in precipitation between CTRL and CLIM was 1.24 mm day^{-1} . Thus, the SM anomalies in May over the ICP region contributed to approximately 10.6% of the precipitation over the YRB in June and July 2020.

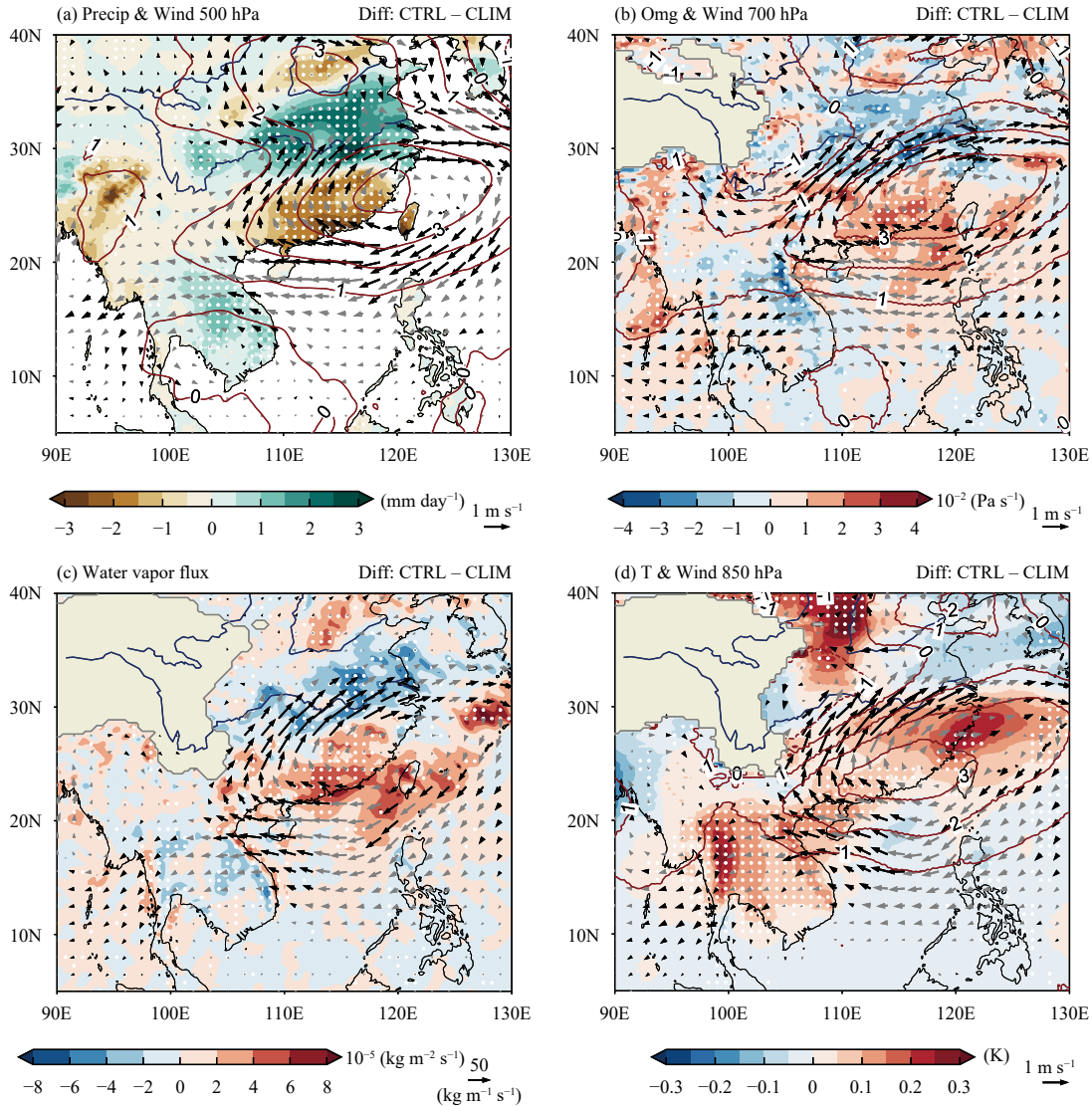


Fig. 8. (a) Daily precipitation (shaded; mm day^{-1}), and 500-hPa wind (vector; m s^{-1}) and geopotential height (red contour; gpm); (b) 700-hPa vertical velocity (shaded; Pa s^{-1}), wind (vector; m s^{-1}), and geopotential height (contour; gpm); (c) water vapor flux (vector; $\text{kg m}^{-2} \text{s}^{-1}$) and its divergence (shaded; $10^{-5} \text{ kg m}^{-2} \text{s}^{-1}$), vertically integrated from 1000 to 300 hPa; (d) 850-hPa temperature (shaded; Pa s^{-1}), wind (vector; m s^{-1}), and geopotential height (contour; gpm), which are obtained by subtracting CLIM from CTRL and averaged from 1 June to 31 July 2020. The black arrows and white dotted areas are significant at the 5% level.

5. Conclusions and discussion

The analytical results of the precipitation observation data, ERA-5 reanalysis data, and various SM data show that the SM anomalies in May in the ICP might have significantly enhanced the precipitation in YRB during the Meiyu period in June and July 2020. The negative SM anomalies in May over the ICP led to surface warming, increased sensible heat flux, and heated the lower troposphere, which increased the geopotential height and facilitated the westward extension of the WPSH. Consequently, the YRB witnessed enhanced southwesterly winds and vertical motion, as well as increased the water

vapor flux and convergence, which were conducive to the occurrence and development of the super Meiyu event in 2020. The SVD results based on recent 30-yr historical data also indicate a significant negative correlation between the SM in May in the ICP and precipitation in June and July over the YRB. The regression results for the wind and geopotential height show the presence of a significant anticyclonic anomaly in Northwest Pacific, which corresponds to the strengthened WPSH. The enhanced anomalous anticyclone was conducive to water vapor convergence and flux over the YRB with southwesterly wind anomalies. The anomaly fields for 2020 agree well with the regression results.

The CTRL run based on the WRF model reproduced the basic characteristics of precipitation and circulation, and the CLIM experiments further confirmed the results of the observational analysis. The differences between CTRL and CLIM show that the negative SM anomalies in the ICP in May 2020 led to an increase in the surface temperature and sensible heat flux, thus heating the lower troposphere. Significant warming occurred in the lower troposphere from the ICP to Northwest Pacific due to background southwesterly winds, which raised the geopotential height, induced an anomalous anticyclone, and increased the temperature gradient over the YRB. Precipitation in the anticyclone-controlled SC decreased; however, the southwesterly flow northwest of the anticyclone induced sufficient water vapor supply and water vapor convergence in the YRB, thereby increasing the precipitation therein. The results of the numerical sensitivity experiments showed that the SM anomalies in May over the ICP could increase the precipitation by 10.6% in the YRB from June to July. The findings of this study can shed light on the formation mechanism of the super Meiyu event in 2020 and provide some reference for the prediction of extreme Meiyu events.

However, this study has some limitations because it only focuses on the physical processes behind the Meiyu event in 2020. The air interaction is often influenced by the SST background and large-scale circulation. Historically, YRB precipitation has often been associated with preceding El Niño events (Feng et al., 2011; Wen et al., 2019). Zhu et al. (2021) found that the effect of spring SM over the ICP on summer precipitation in the YRB varies under different SST backgrounds, and a strong SST background can attenuate the impact of the land surface. Gao et al. (2020a) also indicated that the influence of springtime land surface anomalies on summer precipitation in the YRB has significant interdecadal variability. Since the 1990s, the influence of the land surface has been weakened by abrupt changes in the EASM (Gao et al., 2020c). Thus, further investigation is required to ascertain whether the findings of this study are also applicable to other years of heavy precipitation.

REFERENCES

- Bao, Y. Y., 2021: Similarities and differences of monsoon circulations between 2016 and 1998 Meiyu periods in the middle and lower reaches of the Yangtze River and the comparison of their physical mechanisms. *Chinese J. Atmos. Sci.*, **45**, 994–1006. Available online at <http://www.iapjournals.ac.cn/dqkx/en/article/doi/10.3878/j.issn.1006-9895.2101.20174>. Accessed on 13 March 2023. (in Chinese)
- Bretherton, C. S., C. Smith, and J. M. Wallace, 1992: An intercomparison of methods for finding coupled patterns in climate data. *J. Climate*, **5**, 541–560, doi: [10.1175/1520-0442\(1992\)005<0541:AIOMFF>2.0.CO;2](https://doi.org/10.1175/1520-0442(1992)005<0541:AIOMFF>2.0.CO;2).
- Chen, H. S., X. G. Du, and Y. Sun, 2022: Land surface processes and weather research—a review. *Earth Sci. Front.*, **29**, 382–400, doi: [10.13745/j.esf.2021.9.59](https://doi.org/10.13745/j.esf.2021.9.59). (in Chinese)
- Chow, K. C., Y. M. Liu, J. C. J. Chan, et al., 2006: Effects of surface heating over Indochina and India landmasses on the summer monsoon over South China. *Int. J. Climatol.*, **26**, 1339–1359, doi: [10.1002/joc.1310](https://doi.org/10.1002/joc.1310).
- Dai, Y. J., X. B. Zeng, R. E. Dickinson, et al., 2003: The common land model. *Bull. Amer. Meteor. Soc.*, **84**, 1013–1024, doi: [10.1175/BAMS-84-8-1013](https://doi.org/10.1175/BAMS-84-8-1013).
- Ding, Y. H., and J. C. L. Chan., 2005: The East Asian summer monsoon: An overview. *Meteor. Atmos. Phys.*, **89**, 117–142, doi: [10.1007/s00703-005-0125-z](https://doi.org/10.1007/s00703-005-0125-z).
- Ding, Y.-H., J.-J. Liu, Y. Sun, et al., 2007: A study of the synoptic-climatology of the Meiyu system in East Asia. *Chinese J. Atmos. Sci.*, **31**, 1082–1101, doi: [10.3878/j.issn.1006-9895.2007.06.05](https://doi.org/10.3878/j.issn.1006-9895.2007.06.05). (in Chinese)
- Ding, Y. H., D. Si, Y. J. Liu, et al., 2018: On the characteristics, driving forces and inter-decadal variability of the East Asian summer monsoon. *Chinese J. Atmos. Sci.*, **42**, 533–558, doi: [10.3878/j.issn.1006-9895.1712.17261](https://doi.org/10.3878/j.issn.1006-9895.1712.17261). (in Chinese)
- Ding, Y. H., Y. Y. Liu, and Z. Z. Hu, 2021: The record-breaking Mei-yu in 2020 and associated atmospheric circulation and tropical SST anomalies. *Adv. Atmos. Sci.*, **38**, 1980–1993, doi: [10.1007/s00376-021-0361-2](https://doi.org/10.1007/s00376-021-0361-2).
- Dirmeyer, P. A., C. A. Schlosser, and K. L. Brubaker, 2009: Precipitation, recycling, and land memory: An integrated analysis. *J. Hydrometeor.*, **10**, 278–288, doi: [10.1175/2008JHM1016.1](https://doi.org/10.1175/2008JHM1016.1).
- Dong, X., H. S. Chen, Y. Zhou, et al., 2022a: Local and non-local atmospheric effects of abnormal soil moisture over Indochina during May and June. *Quart. J. Roy. Meteor. Soc.*, **148**, 2903–2926, doi: [10.1002/qj.4341](https://doi.org/10.1002/qj.4341).
- Dong, X., Y. Zhou, H. S. Chen, et al., 2022b: Lag impacts of the anomalous July soil moisture over Southern China on the August rainfall over the Huang-Huai River Basin. *Climate Dyn.*, **58**, 1737–1754, doi: [10.1007/s00382-021-05989-1](https://doi.org/10.1007/s00382-021-05989-1).
- Dorigo, W., W. Wagner, C. Albergel, et al., 2017: ESA CCI soil moisture for improved earth system understanding: State-of-the art and future directions. *Remote Sens. Environ.*, **203**, 185–215, doi: [10.1016/j.rse.2017.07.001](https://doi.org/10.1016/j.rse.2017.07.001).
- Fang, C. X., Y. Liu, Q. F. Cai, et al., 2021: Why does extreme rainfall occur in central China during the summer of 2020 after a weak El Niño? *Adv. Atmos. Sci.*, **38**, 2067–2081, doi: [10.1007/s00376-021-1009-y](https://doi.org/10.1007/s00376-021-1009-y).
- Feng, J., W. Chen, C.-Y. Tam, et al., 2011: Different impacts of El Niño and El Niño Modoki on China rainfall in the decaying phases. *Int. J. Climatol.*, **31**, 2091–2101, doi: [10.1002/joc.2217](https://doi.org/10.1002/joc.2217).
- Gao, C. J., H. S. Chen, B. Xu, et al., 2014: Possible relationships among South China Sea SSTA, soil moisture anomalies in Southwest China and summer precipitation in Eastern China. *J. Trop. Meteor.*, **20**, 228–235, doi: [10.16555/j.1006-8775.2014.03.005](https://doi.org/10.16555/j.1006-8775.2014.03.005).
- Gao, C. J., H. S. Chen, G. Li, et al., 2019: Land–atmosphere interaction over the Indo-China Peninsula during spring and its ef-

- fect on the following summer climate over the Yangtze River basin. *Climate Dyn.*, **53**, 6181–6198, doi: [10.1007/s00382-019-04922-x](https://doi.org/10.1007/s00382-019-04922-x).
- Gao, C. J., G. Li, H. S. Chen, et al., 2020a: Interdecadal change in the effect of spring soil moisture over the Indo-China Peninsula on the following summer precipitation over the Yangtze River basin. *J. Climate*, **33**, 7063–7082, doi: [10.1175/JCLI-D-19-0754.1](https://doi.org/10.1175/JCLI-D-19-0754.1).
- Gao, C. J., G. Li, B. Xu, et al., 2020b: Effect of spring soil moisture over the Indo-China Peninsula on the following summer extreme precipitation events over the Yangtze River basin. *Climate Dyn.*, **54**, 3845–3861, doi: [10.1007/s00382-020-05187-5](https://doi.org/10.1007/s00382-020-05187-5).
- Gao, C. J., G. Li, and B. Xu, 2020c: Weakening influence of spring soil moisture over the Indo-China Peninsula on the following summer Mei-Yu front and precipitation extremes over the Yangtze River basin. *J. Climate*, **33**, 10055–10072, doi: [10.1175/JCLI-D-20-0117.1](https://doi.org/10.1175/JCLI-D-20-0117.1).
- Gu, X. H., J. F. Li, Y. D. Chen, et al., 2019: Consistency and discrepancy of global surface soil moisture changes from multiple model-based data sets against satellite observations. *J. Geophys. Res. Atmos.*, **124**, 1474–1495, doi: [10.1029/2018JD029304](https://doi.org/10.1029/2018JD029304).
- Guo, D., L. W. Wang, Z. K. Li, et al., 2016: Comparison between anomalies of summer rainfall in China in decaying years during super El Niño events of 2015/2016 and 1997/1998. *Trans. Atmos. Sci.*, **39**, 835–844, doi: [10.13878/j.cnki.dqkxxb.20160828010](https://doi.org/10.13878/j.cnki.dqkxxb.20160828010). (in Chinese)
- Hersbach, H., B. Bell, P. Berrisford, et al., 2020: The ERA5 global reanalysis. *Quart. J. Roy. Meteor. Soc.*, **146**, 1999–2049, doi: [10.1002/qj.3803](https://doi.org/10.1002/qj.3803).
- Hong, S. Y., and J. O. J. Lim, 2006: The WRF single-moment 6-class microphysics scheme (WSM6). *J. Korean Meteor. Soc.*, **42**, 129–151.
- Hong, S. Y., Y. Noh, and J. Dudhia, 2006: A new vertical diffusion package with an explicit treatment of entrainment processes. *Mon. Wea. Rev.*, **134**, 2318–2341, doi: [10.1175/MWR3199.1](https://doi.org/10.1175/MWR3199.1).
- Iacono, M. J., J. S. Delamere, E. J. Mlawer, et al., 2008: Radiative forcing by long-lived greenhouse gases: Calculations with the AER radiative transfer models. *J. Geophys. Res. Atmos.*, **113**, D13103, doi: [10.1029/2008JD009944](https://doi.org/10.1029/2008JD009944).
- Koster, R. D., and M. J. Suarez, 2001: Soil moisture memory in climate models. *J. Hydrometeor.*, **2**, 558–570, doi: [10.1175/1525-7541\(2001\)002<0558:SMMC>2.0.CO;2](https://doi.org/10.1175/1525-7541(2001)002<0558:SMMC>2.0.CO;2).
- Lawrence, D. M., K. W. Oleson, M. G. Flanner, et al., 2011: Parameterization improvements and functional and structural advances in version 4 of the Community Land Model. *J. Adv. Model. Earth Syst.*, **3**, M03001, doi: [10.1029/2011MS00045](https://doi.org/10.1029/2011MS00045).
- Li, H. Q., A. Z. Ye, Y. H. Zhang, et al., 2021: Intercomparison and evaluation of multisource soil moisture products in China. *Earth Space Sci.*, **8**, e2021EA001845, doi: [10.1029/2021EA001845](https://doi.org/10.1029/2021EA001845).
- Lin, R. P., J. Zhu, and F. Zheng, 2019: The application of the SVD method to reduce coupled model biases in seasonal predictions of rainfall. *J. Geophys. Res. Atmos.*, **124**, 11837–11849, doi: [10.1029/2018JD029927](https://doi.org/10.1029/2018JD029927).
- Liu, B. Q., Y. H. Yan, C. W. Zhu, et al., 2020: Record-breaking Meiyu rainfall around the Yangtze River in 2020 regulated by the subseasonal phase transition of the North Atlantic Oscillation. *Geophys. Res. Lett.*, **47**, e2020GL090342, doi: [10.1029/2020GL090342](https://doi.org/10.1029/2020GL090342).
- Liu, Y. Y., and Y. H. Ding, 2020: Characteristics and possible causes for the extreme Meiyu in 2020. *Meteor. Mon.*, **46**, 1393–1404, doi: [10.7519/j.issn.1000-0526.2020.11.001](https://doi.org/10.7519/j.issn.1000-0526.2020.11.001). (in Chinese)
- Oleson, K. W., D. M. Lawrence, G. B. Bonan, et al., 2010: Technical Description of Version 4.0 of the Community Land Model (CLM). No. NCAR/TN-478+STR, University Corporation for Atmospheric Research, Boulder, 266 pp, doi: [10.5065/D6FB50WZ](https://doi.org/10.5065/D6FB50WZ).
- Rodell, M., P. R. Houser, U. Jambor, et al., 2004: The global land data assimilation system. *Bull. Amer. Meteor. Soc.*, **85**, 381–394, doi: [10.1175/BAMS-85-3-381](https://doi.org/10.1175/BAMS-85-3-381).
- Seneviratne, S. I., D. Lüthi, M. Litschi, et al., 2006: Land–atmosphere coupling and climate change in Europe. *Nature*, **443**, 205–209, doi: [10.1038/nature05095](https://doi.org/10.1038/nature05095).
- Seneviratne, S. I., T. Corti, E. L. Davin, et al., 2010: Investigating soil moisture–climate interactions in a changing climate: A review. *Earth Sci. Rev.*, **99**, 125–161, doi: [10.1016/j.earscirev.2010.02.004](https://doi.org/10.1016/j.earscirev.2010.02.004).
- Shi, X., J. C. L. Chan, K. C. Chow, et al., 2008: Effects of upstream surface heat fluxes on the evolution of the South China Sea summer monsoon. *Meteor. Atmos. Phys.*, **100**, 303–325, doi: [10.1007/s00703-008-0311-x](https://doi.org/10.1007/s00703-008-0311-x).
- Takaya, Y., I. Ishikawa, C. Kobayashi, et al., 2020: Enhanced Meiyu–Baiu rainfall in early summer 2020: Aftermath of the 2019 super IOD event. *Geophys. Res. Lett.*, **47**, e2020GL090671, doi: [10.1029/2020GL090671](https://doi.org/10.1029/2020GL090671).
- Tao, S. Y., and J. Wei, 2006: The westward, northward advance of the subtropical high over the West Pacific in summer. *J. Appl. Meteor. Sci.*, **17**, 513–525. (in Chinese)
- Wallace, J. M., C. Smith, and C. S. Bretherton, 1992: Singular value decomposition of wintertime sea surface temperature and 500-mb height anomalies. *J. Climate*, **5**, 561–576, doi: [10.1175/1520-0442\(1992\)005<0561:SVDOWS>2.0.CO;2](https://doi.org/10.1175/1520-0442(1992)005<0561:SVDOWS>2.0.CO;2).
- Wang, D. N., C. Menz, T. Simon, et al., 2013: Regional dynamical downscaling with CCLM over East Asia. *Meteor. Atmos. Phys.*, **121**, 39–53, doi: [10.1007/s00703-013-0250-z](https://doi.org/10.1007/s00703-013-0250-z).
- Wang, L. C., X. G. Sun, X. Q. Yang, et al., 2021: Contribution of water vapor to the record-breaking extreme Meiyu rainfall along the Yangtze River valley in 2020. *J. Meteor. Res.*, **35**, 557–570, doi: [10.1007/s13351-021-1030-1](https://doi.org/10.1007/s13351-021-1030-1).
- Wen, N., Z. Y. Liu, and L. Li, 2019: Direct ENSO impact on East Asian summer precipitation in the developing summer. *Climate Dyn.*, **52**, 6799–6815, doi: [10.1007/s00382-018-4545-0](https://doi.org/10.1007/s00382-018-4545-0).
- Yang, K., J. Y. Zhang, L. Y. Wu, et al., 2019: Prediction of summer hot extremes over the middle and lower reaches of the Yangtze River valley. *Climate Dyn.*, **52**, 2943–2957, doi: [10.1007/s00382-018-4302-4](https://doi.org/10.1007/s00382-018-4302-4).
- Zhang, C. X., and Y. Q. Wang, 2017: Projected future changes of tropical cyclone activity over the western North and South Pacific in a 20-km-Mesh Regional Climate Model. *J. Climate*, **30**, 5923–5941, doi: [10.1175/JCLI-D-16-0597.1](https://doi.org/10.1175/JCLI-D-16-0597.1).
- Zhang, F. H., T. Chen, F. Zhang, et al., 2020: Extreme features of severe precipitation in Meiyu period over the middle and lower reaches of Yangtze River basin in June–July 2020. *Meteor. Mon.*, **46**, 1405–1414, doi: [10.7519/j.issn.1000-0526](https://doi.org/10.7519/j.issn.1000-0526).

2020.11.002. (in Chinese)

- Zhang, L. X., D. Zhao, T. J. Zhou, et al., 2021: Moisture origins and transport processes for the 2020 Yangtze River valley record-breaking Mei-yu rainfall. *Adv. Atmos. Sci.*, **38**, 2125–2136, doi: [10.1007/s00376-021-1097-8](https://doi.org/10.1007/s00376-021-1097-8).
- Zhang, R. H., and Z. Y. Zuo, 2011: Impact of spring soil moisture on surface energy balance and summer monsoon circulation over East Asia and precipitation in East China. *J. Climate*, **24**, 3309–3322, doi: [10.1175/2011JCLI4084.1](https://doi.org/10.1175/2011JCLI4084.1).
- Zhang, W. J., Z. C. Huang, F. Jiang, et al., 2021: Exceptionally persistent Madden–Julian Oscillation activity contributes to the extreme 2020 East Asian summer monsoon rainfall. *Geophys. Res. Lett.*, **48**, e2020GL091588, doi: [10.1029/2020GL091588](https://doi.org/10.1029/2020GL091588).
- Zhang, Y., Z. Y. Meng, P. J. Zhu, et al., 2016: Mesoscale modeling study of severe convection over complex terrain. *Adv. Atmos. Sci.*, **33**, 1259–1270, doi: [10.1007/s00376-016-5221-0](https://doi.org/10.1007/s00376-016-5221-0).
- Zhou, Z. Q., S. P. Xie, and R. H. Zhang, 2021: Historic Yangtze flooding of 2020 tied to extreme Indian Ocean conditions. *Proc. Natl. Acad. Sci. USA*, **118**, e2022255118, doi: [10.1073/pnas.2022255118](https://doi.org/10.1073/pnas.2022255118).
- Zhu, S. G., Y. J. Qi, H. S. Chen, et al., 2021: Distinct impacts of spring soil moisture over the Indo-China Peninsula on summer precipitation in the Yangtze River basin under different SST backgrounds. *Climate Dyn.*, **56**, 1895–1918, doi: [10.1007/s00382-020-05567-x](https://doi.org/10.1007/s00382-020-05567-x).
- Zhuang, M. R., A. M. Duan, R. Y. Lu, et al., 2022: Relative impacts of the orography and land–sea contrast over the Indochina Peninsula on the Asian summer monsoon between early and late summer. *J. Climate*, **35**, 3037–3055, doi: [10.1175/JCLI-D-21-0576.1](https://doi.org/10.1175/JCLI-D-21-0576.1).

Tech & Copy Editor: Mengyuan CHEN